energies

MDPI

Article

Synthesis of $LiNi_{0.85}Co_{0.14}Al_{0.01}O_2$ Cathode Material and its Performance in an NCA/Graphite Full-Battery

Cornelius Satria Yudha [1], Soraya Ulfa Muzayanha [1], Hendri Widiyandari [2,3], Ferry Iskandar [3,4], Wahyudi Sutopo [3,5] and Agus Purwanto [1,3,*]

1 Department of Chemical Engineering, Faculty of Engineering, Universitas Sebelas Maret, Jl. Ir. Sutami 36 A, Surakarta, Central Java 57126, Indonesia; cornelyudha@student.uns.ac.id (C.S.Y.); sorayamuzayanha@student.uns.ac.id (S.U.M.)
2 Department of Physics, Faculty of Mathematic and Natural Science, Universitas Sebelas Maret, Jl. Ir. Sutami 36 A, Surakarta, Central Java 57126, Indonesia; hendriwidiyandri@staff.uns.ac.id
3 National Center for Sustainable Transportation Technology, Institut Teknologi Bandung, Jl. Ganesha No.10, Bandung, West Java 40132, Indonesia; ferry@fi.itb.ac.id (F.I.); sutopo@uns.ac.id (W.S.)
4 Department of Physics, Institut Teknologi Bandung, Jl. Ganesha No.10, Bandung, West Java 40132, Indonesia
5 Department of Industrial Engineering, Faculty of Engineering, Universitas Sebelas Maret, Jl. Ir. Sutami 36 A, Surakarta, Central Java 57126, Indonesia
* Correspondence: aguspur@uns.ac.id

Received: 22 April 2019; Accepted: 13 May 2019; Published: 17 May 2019

Abstract: Nickel-rich cathode material, NCA (85:14:1), is successfully synthesized using two different, simple and economical batch methods, i.e., hydroxide co-precipitation (NCA-CP) and the hydroxides solid state reaction method (NCA-SS), followed by heat treatments. Based on the FTIR spectra, all precursor samples exhibit two functional groups of hydroxide and carbonate. The XRD patterns of NCA-CP and NCA-SS show a hexagonal layered structure (space group: R_3m), with no impurities detected. Based on the SEM images, the micro-sized particles exhibit a sphere-like shape with aggregates. The electrochemical performances of the samples were tested in a 18650-type full-cell battery using artificial graphite as the counter anode at the voltage range of 2.7–4.25 V. All samples have similar characteristics and electrochemical performances that are comparable to the commercial NCA battery, despite going through different synthesis routes. In conclusion, the overall results are considered good and have the potential to be adapted for commercialization.

Keywords: synthesis; Li-ion batteries; electrochemical performance; NCA

1. Introduction

Current technology for energy storage has shifted from conventional lead acid batteries to lithium-ion batteries (LIBs) due to the rapid increase of electronic devices which require high energy and power density power sources [1,2]. Intercalation cathode material in LIBs is the most important factor determining the cell's performance, thus most studies have been focused on the development of such material and performance enhancement efforts. Lithium transitional metal oxide, such as $LiCoO_2$ (LCO), has been widely used for intercalation cathodes since the late 20th century. However, the fact that it is highly toxic, expensive, and thermally unstable, and has a poor rate ability during extensive cycling are the shortcomings of LCO. On the other hand, extensive cobalt exploitation may result in geopolitical and humanity issues [3]. Reducing the cobalt content while increasing cheaper and more available materials such as nickel (Ni) has been discussed in the past twenty years [4]. Ni-rich cathode materials enjoy the advantages of a high capacity and high power density due to their relatively high potential vs. Li (3.7 V). This situation is extremely important for designing high-performance

LIBs. For example, nickel-rich cathode material (NCA) ($LiNi_xCo_yAl_zO_2$) batteries have been applied to TESLA Electric Vehicles (EVs) due to their superior performance and lower price compared to commercially established LCO batteries [5,6].

Various methods of obtaining NCA cathode powders have been performed by researchers. Direct solid state synthesis of NCA is the most simple and scalable method for mass powder production; however, the obtained powder exhibits poor atomic homogeneity despite multiple ball milling processes, a higher sintering temperature, and a longer sintering time being applied [7,8]. To overcome the inhomogeneous composition, a wet route such as sol-gel [9,10] and the spray method [11–13] were employed. Although particles with a unique morphology were obtained, these methods involve costly organic and flammable material which increases safety concerns, so large-scale adaptation is hindered [4,14]. Recently, the co-precipitation process of an NCA precursor (hydroxide and carbonate), followed by solid state lithiation, has become the preferred method for producing NCA commercially [15–17]. This method is also used in the functionalization, doping, and surface modification (coating) of NCA powders [18–21]. Major advantages of the co-precipitation method are: it does not require sophisticated technology; any raw material can be used, as long as it dissolves easily in the solvent; it has a mild operation condition; and it produces spherical secondary particles with a narrow size distribution. Recent studies on continuous co-precipitation have produced satisfying results [22–25]. However, extensive control of pH, flow rate, agitation, and temperature has become the main problem in developing the method. On the other hand, such a method requires a long reaction and aging time, which is unfavorable for industrialization. Thus, a facile, inexpensive, and simple route to obtain NCA cathode material is greatly needed.

In this study, we performed batch syntheses of nickel-rich NCA ($LiNi_{0.85}Co_{0.14}Al_{0.01}O_2$) using the solid state method and co-precipitation methods, as efforts to reduce the complexity of the continuous process stated before. The solid state reaction was performed by heating pre-milled starting materials. Unlike previous studies, metal hydroxides as raw materials are chosen rather than metal oxides due to their similar sintering behavior to the precursor obtained from co-precipitation. Batch hydroxide co-precipitation was carried out using technical grade materials such as Li, Ni, Co, and Al sources; ammonia as the chelating agent; and NaOH as the precipitant. To the best of our knowledge, such approaches have never been reported. The electrochemical performance of the products was analyzed in a full-cell 18650-type battery using graphite as the commercial counter anode. The charge-discharge performance of NCA samples and commercial NCA is comparable. This situation provides strong evidence that such methods are suitable for mass production and commercialization.

2. Materials and Methods

2.1. Material Synthesis

NCA powders were obtained using two different routes. NCA powders obtained by the solid-state method (NCA-SS) were obtained by mixing solid materials of LiOH (merck, Germany), $Ni(OH)_2$ (merck, Germany), $Co(OH)_2$ (merck, Germany), and $Al(OH)_3.H_2O$ (merck, Germany) using a ball mill for 3 h in ethanol medium (1:1 *w*/*w*). The hydroxide composite (NCA-PSS) was calcined at 450 °C under air for 6 h and sintered at 800 °C under oxygen flow of 2 L/min for 12 h.

For the hydroxide precursor, 100 ml of 2 M of technical grade $NiSO_4.6H_2O$ (Zenith, Brazil), $CoSO_4.7H_2O$ (Rubamin, India), and $Al_2(SO4)_3.18H_2O$ (Indoacid, Indonesia) with a molar ratio of Ni:Co:Al = 85:14:1 was mixed with 100 ml of 1 M NH_4OH inside a three-necked round bottom flask and heated to 60 °C for half an hour to form a stable metal ions complex. Separately, 150 ml of 4 M NaOH (Asahi, Indonesia) solution was also heated to 60 °C. Both solutions were mixed together to form a greenish precipitate. The stirring speed and temperature were maintained at 600 rpm and 60 °C using an overhead mixer and water bath, respectively. The pH of the solution was monitored using a calibrated pH meter and maintained at the level of 10–11. After 6 h of mixing and monitoring, the temperature was cooled down to room temperature while the stirring was maintained for twelve hours.

The precipitates were filtered and washed three times using hot demineralized water and once with alcohol, followed by drying in the oven for 3 h. The powder was denoted as NCA-PCP. The powders were mixed thoroughly with LiOH with an excess mole of 5% using a mortar and pestle and calcined at 450 °C for 6 h under air followed by sintering at 800 °C for 12 h under oxygen flow of 2 L/min. The NCA powder obtained from NCA-OH was denoted as NCA-HC. The overview of each process is presented in Table 1.

Table 1. Overview of each process.

Parameter	Solid State Method	Hydroxide Co-Precipitation
Materials	Metal hydroxides	Metal sulfate and LiOH
Chelating Agent	-	NH3.H2O
Precipitant	-	NaOH
Precipitation time	-	6 h
Aging time	-	12 h
Milling time	3 h	30 min
Heat treatment	20 h	20 h

2.2. Material Characterization

The crystal structure of the products was analyzed using an X-Ray Diffractometer (D2 Phaser Bruker, Germany) employing CuKα radiation λ = 1.54 Å with a 2θ range of 10–80° and scan-rate of 0.02° per second. The morphology of the sample was analyzed using a Scanning Electron Microscope (SEM) (JEOL JSM-6510LA, Japan). The Ni, Co, and Al elements in the powder were analyzed using X-Ray Fluorescence (Bruker XRF Spectrometer, Germany). The functional groups and surface composition of the precursors and as-prepared samples were analyzed using Fourier Transformed Infrared Spectroscopy (FTIR Spectroscopy) (Shimadzu FTIR Spectrometer, Japan).

2.3. Electrochemical Performance Test

The electrochemical performance was tested using a cylindrical full cell (18650) utilizing artificial graphite or mesocarbon microbeads (MCMB) (MTI, America) as the counter anode. The acetylene black (AB) and polyvinylidene fluoride (PVDF) (MTI, America) were used as a conductive agent and binder, respectively. To assure full Li-ion transfer, the cathode was chosen as the limiting electrode; therefore, it was selected as the basis mass of calculation. The cathode slurry was prepared by mixing NCA samples with AB and PVDF with the ratio of NCA:AB:PVDF = 92:3:5 in N-Methyl-2-pyrrolidone (NMP) solvent. The slurry was subsequently cast on both sides of aluminum (Al) foil using a doctor blade with the thickness of 150 μm and dried in an oven at 120 °C for 1 h. The dried cathode was transferred to a vacuum oven and dried at 80 °C for 12 h. The counter anode slurry was prepared by MCMB, AB, and PVDF with the ratio of MCMB:AB:PVDF = 92:3:5 in NMP solvent. The anode slurry was cast on both sides of copper (Cu) foil with a thickness of 100 μm and dried in vacuum for 12 h. The cathode and anode sheet were pressed and silted. The calculated mass loading of the cathode and anode was 30 mg/cm^2 and 24 mg/cm^2, respectively. The edge of the cathode and anode were welded with an Al and Ni tab, respectively. Both welded electrodes along with polypropylene separator (MTI, America) were rolled using a winding machine (MSK-112A, MTI) and assembled in a cylindrical case, while the electrolyte (1 M $LiPF_6$ in Ethylene Carbonate (EC):Diethyl Carbonate (DEC):Dimethyl Carbonate (DMC)=1:1:1, *v*/*v* (MTI, China)) filling was performed inside ab argon-filled glovebox. After the cell was assembled, the cell was aged for a day before the electrochemical performance was tested. The charge-discharge performance was tested using an NEWARE Battery analyzer and BTS software with a voltage window of 2.7–4.25 V at 0.05 C or 10 mA/g (1 $C_{theoretical}$ = 200 mA/g). The first three cycles were considered as formation cycles, while the capacity of the cell was determined from the next cycle. The rate and cycle performances were carried out based on the true capacity of the

cell. As a comparison, a battery using commercial NCA (BTR, China) as the cathode and MCMB (MTI, America) was fabricated and tested.

3. Results and Discussion

3.1. NCA Precursor Characterization

Figure 1 shows the FTIR spectra of precursors from each process, namely NCA-PCP and NCA-PSS. The absorbance spectra of NCA-PCP and NCA-PSS samples show similar results to those of studies by Agarwal et al. on Ni nanoplates [26], Motlagh et al. on Ni(OH)/NiO nanoparticles [27], and Seo et al. on $Li(Ni_{0.8}Co_{0.16}Al0._{04})O_2$ materials [15]. The sharp peak around the value of 3600/cm and the broad peak around the value 3400/cm indicate a stretching mode of the disturbed hydroxide group and stretching vibration of the free hydroxide group, which correspond strongly to the presence of metal hydroxide species ($Ni(OH)_2$). The peak around 1600/cm indicates the bending mode of water molecule vibration, while the peak around 1400/cm indicates a CO_3^{2-} stretching band, so it could be concluded that the sample contained carbonate and water species due to the direct contact of sample powders with air during the preparation. Double peaks which occurred in NCA-PSS were caused by the presence of LiOH in the composite, which is easily converted to Li_2CO_3 under an atmospheric condition. As a result, sample NCA-PSS has a stronger carbonate peak compared to NCA-PCP. Based on Figure 1, the co-precipitation of the hydroxide precursor using technical grade starting materials shows no observable oxide impurities, which often occurs during atmospheric co-precipitation of Co in a highly alkaline solution [28]. The oxidation of Co is prevented due to the de-aeration process before the co-precipitation process occurs.

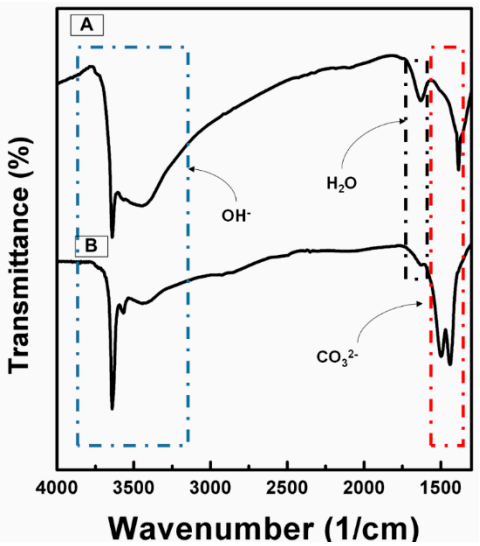

Figure 1. FTIR Spectra of the (**A**) NCA-PCP sample and (**B**) NCA-PSS sample.

3.2. NCA Samples Characterization

Both samples were heat treated evenly using the same procedure, which was a calcination and sintering process. To assure the structural quality of NCA samples, the samples were analyzed using XRD. Figure 2 presents the XRD patterns of as-prepared NCA samples after heat treatment. It is clear that all samples exhibit a layered α-$NaFeO_2$-like hexagonal structure (space group: R_3m). Highly crystalline peaks are in good agreement with The Joint Committee on Powder Diffraction Standards (JCPDS) card no. 87-1562, with no observable impurities phase. The peak splits of 006/102 and 018/110 could be clearly observed in both samples, hence it could be concluded that the NCA-PC and NCA-SS have a well-ordered layered structure [8,29,30]. As it has been predicted before, the use of hydroxide starting materials in a conventional solid state method will result in better mixing and

homogenization of material, which does not require multiple milling and a long sintering time, as well as special tools, like in previous studies [7,8,30,31]. A well-ordered degree of layered material could be evaluated using the lattice parameters and R value. The lattice parameters of each product were calculated using the least square regression method. The crystallite size of each sample was obtained via the Debye–Scherrer equation utilizing the full width at half maximum (FWHM). Both lattice parameters and crystallite size are listed in Table 2. It is clearly shown that the c/a value of both samples is above 4.899, which, according to Zhu et al., means that the sample exhibits a more ordered layered structure. In addition, the R value of both samples is below 0.45, which indicates good hexagonal ordering of the lattice [32].

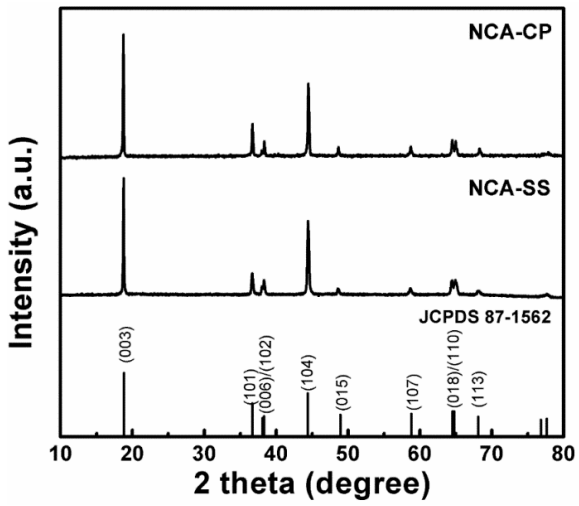

Figure 2. XRD patterns of NCA samples prepared by batch co-precipitation (NCA-CP) and the solid state reaction method (NCA-SS).

The presence of Ni^{2+} which occurs during phase formation could negatively affect the performance of NCA cathode material, mainly due to its similar radii, with Li atomic radii resulting in the substitution of Li with Ni^{2+}. A stable Ni^{2+} ion is very hard to oxidize, which will block the Li-ion pathway, so its intercalation and de-intercalation process is hindered, resulting in a poor electrochemical performance. Such a phenomenon is called cation mixing and its degree or level could be indicated by evaluation of the I003/I104 value. The intensity ratio of I003/I104 listed in Table 2 strongly depends on the method. Based on previous studies on Ni-rich cathode material, the higher the value of I003/I104, the lower the cation mixing level of the material [15,30,33,34].

Table 2. Lattice parameters of as-prepared samples.

Variable	c/a	Cell Volume (Å ^{3})	Crystallite Size (nm)	I003/I104	R (I006/(I101 + I012))
NCA-CP	4.934	100.602	73.6	1.541	0.405
NCA-SS	4.921	101.102	74.4	1.652	0.423

The surface composition of the NCA samples is conducted by analyzing the FTIR spectrum measurement, as shown in Figure 3. It can be clearly seen that the carbonate compound is found on the surface of the sample (860/cm, 1492/cm, and 1499/cm), which could be attributed to Li_2CO_3 as a result of excess Li source [35,36]. During the heating process, hydroxide and carbonate species, as confirmed in Figure 1, are decomposed into H_2O and CO_2, while residual LiOH is converted into Li_2CO_3, so the former peaks are observable, while the LiOH peak is hardly noticeable. Previous studies have suggested performing washing of the obtained NCA powders; however, washing such material using demineralized water may cause structural change, e.g., an inactive rock-salt structure, and

to overcome such phenomena requires a reheating process at a high temperature that is considered uneconomical [36]. Therefore, we decided not to perform any further treatments of the samples.

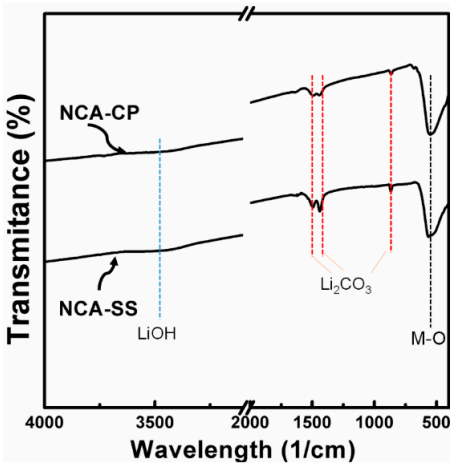

Figure 3. FTIR spectra of the NCA-CP sample and NCA-SS sample.

Figure 4 presents SEM images of as-prepared samples at various magnifications. From the figure, all samples have nano-sized to submicron-sized primary particles which agglomerate to form larger spherical secondary particles. NCA-SS secondary particles show a smoother morphology and denser sphere compared to NCA-CP particles due to the morphology of raw materials, especially $Ni(OH)_2$, which also has a spherical shape. The tapped density of NCA-CP is 1.93 g/cm^3, while the tapped density of NCA-SS is 2.17 g/cm^3. The starting materials could maintain their shape and morphology during the synthesis process, while previous studies of the solid state method using similar material have shown different morphologies of the finished product due to multiple grinding processes [7,8]. NCA-CP has a lower density compared to NCA-SS, which may be affected by the process during the batch co-precipitation. The presence of Al^{3+} ions may hinder the formation of dense secondary particles due to the natural amphoteric habit of Al^{3+}, thus, during the precipitation, precipitated Al may dissolve into sodium aluminate, making the secondary particle less spherical compared to previous studies [22,23].

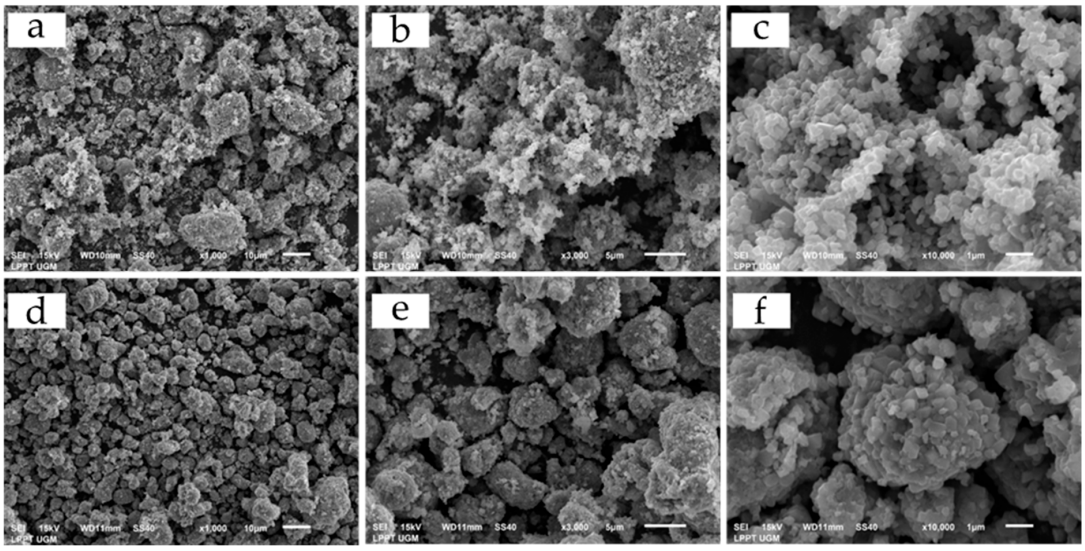

Figure 4. SEM images of (**a**) NCA-CP at 1000× magnification, (**b**) NCA-CP at 3000× magnification, (**c**) NCA-CP at 10,000× magnification, (**d**) NCA-SS at 1000× magnification, (**e**) NCA-SS at 3000× magnification, (**f**) NCA-CP at 10,000× magnification.

Further particle analysis was conducted using a statistical method and the results are presented in Figure 5. Based on Figure 4a,d, the size of the secondary particles is collected and classified into grouped data. NCA-CP and NCA-SS have a similar narrow particle size distribution. The average sizes of the particles, D10, D50, and D90, are shown in Table 3. The D50, or the median, has been defined as the diameter where half of the population lies below this value. Accordingly, 90% of the distribution lies below the D90, and 10% of the population lies below the D10. NCA-CP samples have a relatively smaller average diameter compared to previous studies that used the continuous co-precipitation method [22–25], which, as predicted before, could be caused by aluminum ion dissolution at a high pH, which hinders particle growth [17,37]. However, smaller-sized particle have advantages such as a larger surface area and faster Li-ion diffusion compared to particles with a larger size.

Table 3. Particle size analysis.

Sample	Average Diameter (μm)	D10 (μm)	D50 (μm)	D90 (μm)
NCA-CP	3.961	0.994	3.301	7.615
NCA-SS	3.773	1.173	3.518	6.638

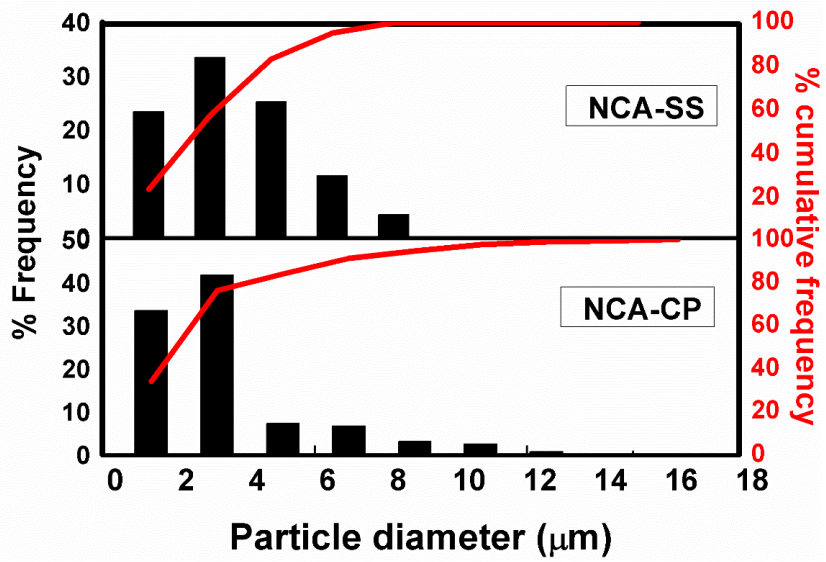

Figure 5. Particle size histogram.

The atomic compositions of Ni, Co, and Al examined by XRF of all samples are listed in Table 4. It is clearly shown that Ni composition is about 83–86% among the ternary metal, which is similar to the targeted value of 85%, while the Al atom composition is far less than 1%. It is predicted that in sample NCA-CP, the Al ion is difficult to precipitate, which largely depends on the pH of the reaction. Since the precipitation involves the formation of solid in the presence of precipitant such as OH^- ions, the process largely depends on the Ksp value of the metals. Ksp is a solubility product constant. Thus, its value can predict the occurance of precipitation [23,38]. The $Al(OH)_3$ precipitation occurs faster than Co and Ni due to its extremely low Ksp value (log Ksp $Al(OH)_3$ = –32.34) compared to the Ksp value of Co (log Ksp $Co(OH)_2$= –14.8) and Ni hydroxide (log Ksp $Ni(OH)_2$= –14.7) [37]. When the $Al(OH)_3$ is formed, $Ni(OH)_2$ and $Co(OH)_3$ have not yet formed. This initiates a large amount of $Al(OH)_3$ nuclei, so the formation of smaller particles continuously occurs while the growth of the existing nuclei into larger particles is hindered [16]. In addition, to promote larger crystal growth, the pH of the solution is elevated. However, when the pH is larger than 11, precipitated $Al(OH)_3$ will dissolve, forming aluminate ions.

Table 4. Molar fraction of the ternary metal of as-prepared NCA samples.

Samples	Molar Fraction (mol%)		
	Ni	Co	Al
NCA-HC	0.8362	0.1598	0.0040
NCA-SS	0.8537	0.1373	0.0090

3.3. Electrochemical Performance Test

The electrochemical performance of the samples was tested in a 18650-type full battery using commercial graphite/Mesocarbon microbeads (MTI, America) as the counter anode instead of novel anodes [39,40]. Such an approach is seldom reported in research papers, yet provides better evidence for material commercialization. The charge-discharge curves obtained at 1/20 C of each sample and commercial NCA (labelled as NCA-Com) are shown in Figure 6. Additional information regarding the NCA-Com characterization is provided in the Appendix A, specifically Figures A1–A3, and Table A1. The first three cycles of the battery test are considered the formation phase. The first cycle performance of three cells is listed in Table 5. In the formation phase, the coulombic efficiency of NCA-CP, NCA-SS, and NCA-Commercial is 69.36%, 69.19%, and 72.97%, respectively. About 30% capacity loss is attributed to solid electrolyte interphase (SEI) formation on both the cathode and anode side. The difference of NCA-CP and NCA-SS coulombic efficiency is insignificant; however, the value is slightly lower than the commercial NCA. The initial specific discharge capacity of NCA-SS and NCA-CP is similar; however, the value is also slightly lower than the commercial NCA. This situation might be caused by the morphology characteristics of as-prepared samples. The smaller secondary particles followed by a large amount of aggregates have a larger surface area, thus promoting side reactions between the materials with the electrolyte during the first charge. These side reactions might form a passivation layer, resulting in irreversibility in electrochemical performances [30,41,42]. In a study by Hsieh et al. [31], the low capacity and high irreversibility level on NCA cathode material were caused by the high amount of aggregates present during the synthesis and defect in the lattice. The initial specific discharge capacity of each cell is considered as the actual capacity and later denoted as C′. Therefore, the value of the 1 C′ rate of NCA-CP, NCA-SS, and NCA-Com is 126.1 mA/g, 129.1 mA/g, and 135.03 mA/g, respectively.

Table 5. Initial charge-discharge performance of NCA samples.

Samples	Formation at 1/20 C (1 C = 200 mA/g)		
	Specific Charge Capacity (mAh/g)	Specific Discharge Capacity (mAh/g)	Coulombic Efficiency
NCA-CP	181.75	126.10	69.36%
NCA-SS	186.72	129.15	69.19%
NCA-Com	185.13	135.03	72.92%

The rate-ability of NCA samples is shown in Figure 7 using a standard testing procedure in which the charging and discharging rates were set using the actual capacity presented in Table 5 (C′) rather than the theoretical capacity (C). After the cells went through the formation phase for five cycles, the cells were charged at 0.5 C′ and discharged at various discharging rates. Based on Figure 7, sample NCA-SS and NCA-CP have a similar rate performance behavior and are relatively comparable to commercial NCA. Surprisingly, at a higher rate, NCA-SS and NCA-CP are superior compared to commercial NCA. Such a phenomenon occurred due to the higher surface area of the as-prepared samples. At high current rates, the performance of cells depends on the Li ion mass transfer and diffusion kinetics. Therefore, even though a large surface area promotes side reactions, it becomes beneficial during a high rate discharging process [17]. To prove the reversability of the material, the

cells were charged and discharged using the first rate (10 mA/g or 0.05 C). From the figure, it appears that all samples exhibit a small capacity drop, even after being discharged at high current rates.

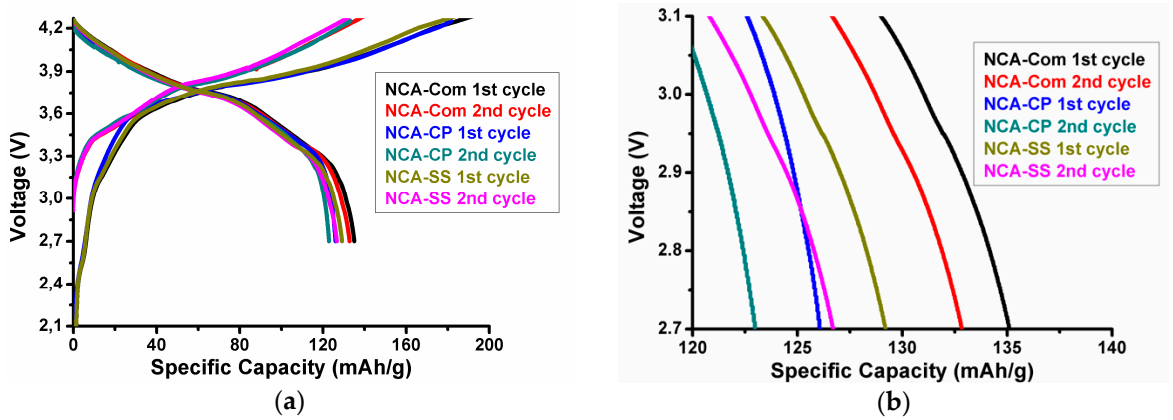

Figure 6. (**a**) Charge-discharge curve of NCA-CP, NCA-SS and NCA-Com during the first and second cycle and (**b**)Specific discharge curve of NCA-CP, NCA-SS and NCA-Com Zoomed at 2.7 V

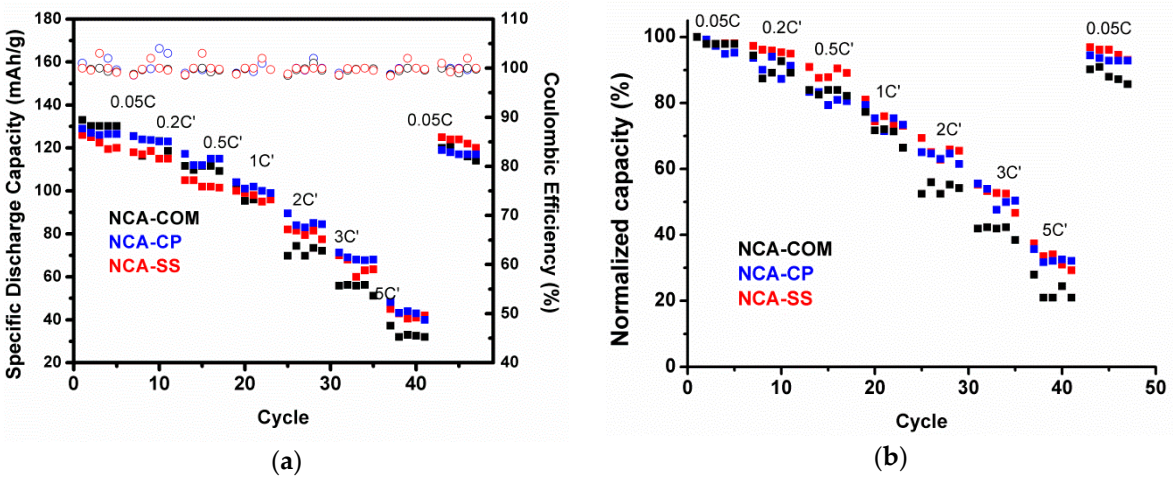

Figure 7. (**a**) Rate performance and (**b**) the normalized rate performance of NCA-CP, NCA-SS and NCA-Com in a 18650-type full battery.

Figure 8a shows the cycle performance of NCA-CP and NCA-SS, respectively. The normalized capacity in Figure 8b refers to the actual capacity, the initial capacity, of each sample. NCA-CP and NCA-SS have similar cycling behaviors for 100 cycles at 1 C' rates and have a capacity retention of 84.4% and 86.3%, respectively. The capacity drop occurred during the initial cycles; however, after three to four cycles, the capacity is considered stable after 100 cycles. The capacity drop phenomena is similar to the study result of Zhang et al., hence the capacity drop of samples in the NCA-battery resulted from impedance rising and cell polarization [43]. Overall, the cycle performance of NCA-CP and NCA-SS is comparable to the commercial NCA. Major problems in NCA commercialization rely on the synthesis methods. Based on the electrochemical performance test results, more feasible, scalable, and commercially attractive methods, such as facile batch co-precipitation and the solid state method, could produce NCA cathode material with comparable performances to commercial NCA which is produced by a continous co-precipitation process. In addition, the use of technical grade raw materials in NCA-CP provides stronger evidence on the merits of the method. Overall, NCA-SS shows a slightly better performance compared to NCA-CP. The higher I003/I104 value based on the XRD pattern and better morphology according to the SEM result might be the reasons behind the difference in the performance, specifically in terms of the capacity.

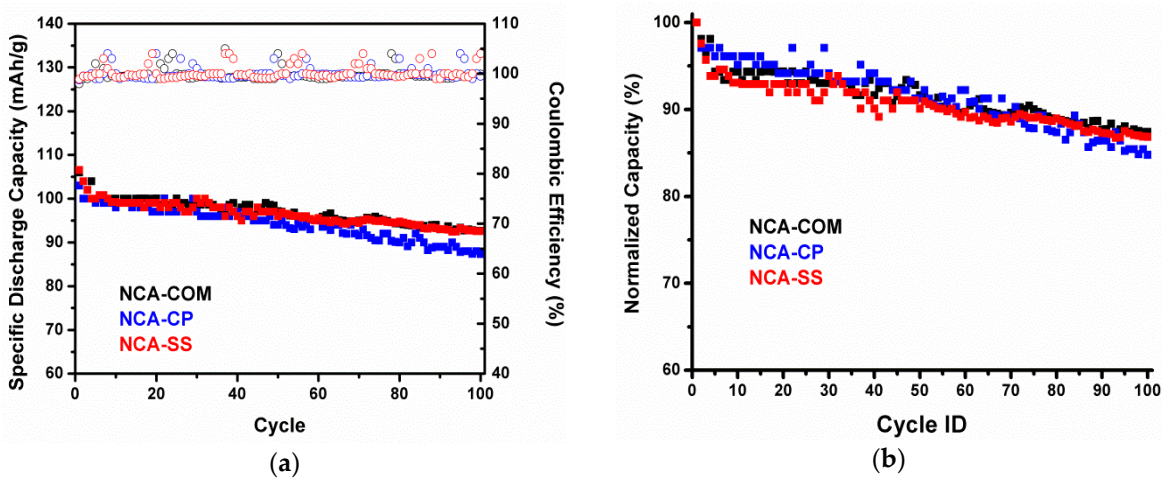

Figure 8. (**a**) Cycle performance and (**b**) the normalized cycle performance of NCA-CP, NCA-SS and NCA-Com in 18650-type batteries in 1 C′.

Post-structural analysis was performed to investigate the reason for low capacity loss during the first cycle. The XRD patterns of the NCA-CP pre-cycle and post-cycle are displayed in Figure 9. From the figure, impurities are clearly observed at two theta around 20–32°, which could be indexed with Li_2CO_3 (JCPDS card no. 87-0729). The formation of Li_2CO_3 or other carbonate compounds such as $ROCO_2Li$ occurred due to side reactions between the electrolyte and the cathode material promoted by the large surface area of aggregates, confirming previous results [31,35,42]. The post-cycle sample patterns have a broader peak compared to the pre-cycle sample, which indicates a decrease in crystallinity; however, the layered structure of the NCA sample is not altered after cycling and is proven by lattice parameter analysis listed in Table 6. The sample exhibits a slight cell volume change (less than 1 $Å^3$) after the cycle and slight decrease in the I003/I104 ratio, which indicates a rigid structure and minimum Li^+/Ni^{2+} mixing in the lattice, respectively, resulting in a good cycle-ability and reversibility during rate performance.

Table 6. Pre-cycle and post-cycle analysis of NCA-HC.

Variable	c/a	Vol ($Å^3$)	I003/I104	R (I006/(I101+I012))
NCA-HC Pre-cycle	4.934	100.602	1.541	0.405
NCA-HC Post-cycle	4.963	100.703	1.463	0.384

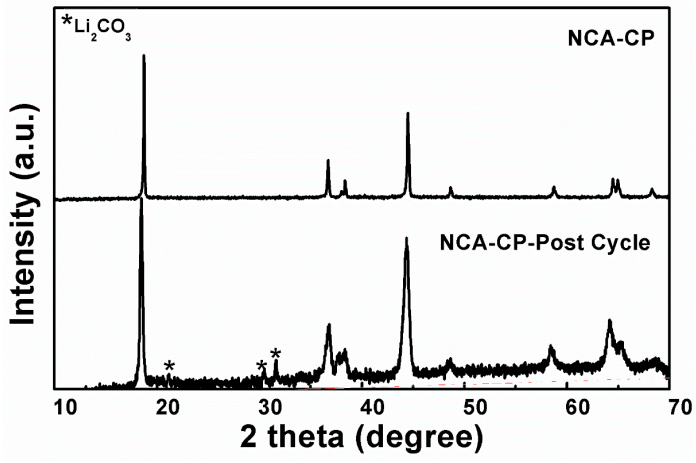

Figure 9. XRD Patterns of NCA-HC before and after cycling.

4. Conclusions

Batch syntheses of $LiNi_{0.85}Co_{0.14}Al_{0.01}O_2$ cathode material are performed via co-precipitation and the solid-state method. Based on the structural analysis, well-ordered layered hexagonal structured material is successfully synthesized. The SEM analysis proved that sphere-like particles are obtained via a solid state reaction and hydroxide co-precipitation reaction. Although exhibiting a narrow particle distribution, both samples also have small particle sizes, which caused larger capacity loss during the first cycle compared to commercial NCA due to a parasitic side reaction between the delithiated cathode material and the electrolyte, which is confirmed by post-structure analysis. The initial discharge capacity of NCA-CP, NCA-SS, and commercial NCA is 126.1, 129.15, and 135.03 mAh/g, respectively, while the capacity retention after being cycled at 1 C′ for 100 cycles is 84.4, 86.3, and 87.1%, respectively. The galvanostic tests proved that the as-prepared samples have a similar good performance, regardless of the synthesis methods. However, future development of the optimization of process variables is necessary in order to obtain better characterized material. The overall result of both the physico-chemical characteristic and electrochemical characteristic could be considered good and promising in terms of adaptation for mass production considering that the layered NCA material could be obtained via simple and economical batch synthesis.

Author Contributions: Conceptualization, H.W., F.I., and W.S.; Data curation, C.S.Y.; Formal analysis, C.S.Y.; Investigation, S.U.M., H.W., F.I., and W.S.; Methodology, C.S.Y.; Project administration, A.P.; Supervision, A.P.; Validation, H.W., F.I., and W.S.; Visualization, S.U.M.; Writing—original draft, C.S.Y.; Writing—review & editing, A.P.

Funding: This research was funded by the Ministry of Research, Technology and Higher Education (KemenRistekdikti) through the Penelitian Hibah Kompetensi scheme (Contract number: 474/UN27.21/PP/2018) and PT PERTAMINA.

Acknowledgments: Cornelius S. Yudha is thankful for the Master Program Scholarship provided by Sebelas Maret University.

Conflicts of Interest: There are no conflicts of interest to declare.

Appendix A

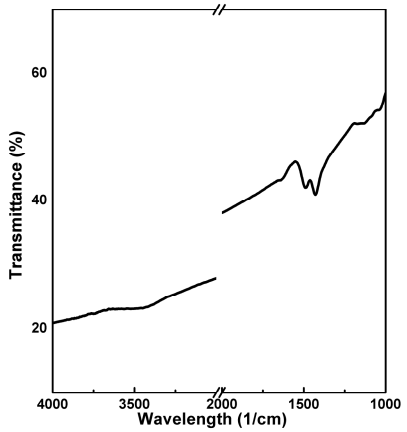

Figure A1. FT-IR Spectra of Commercial NCA (BTR, China).

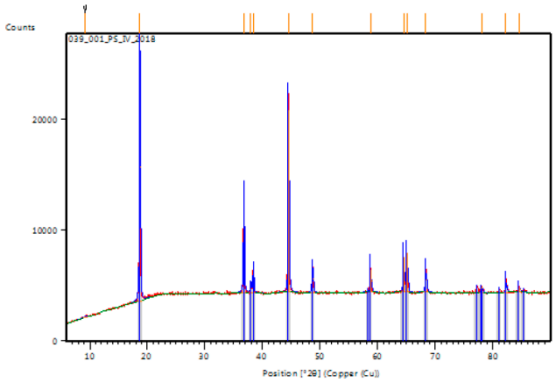

Figure A2. XRD patterns of Commercial NCA (BTR, China).

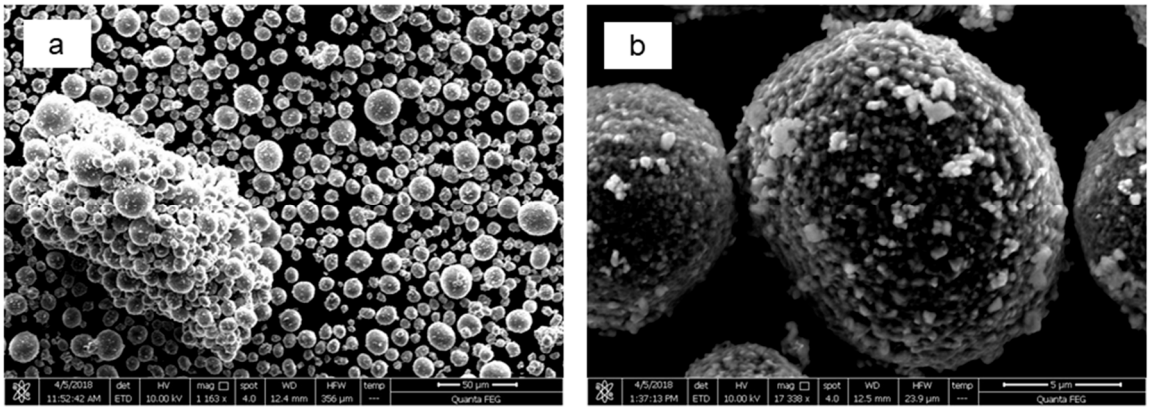

Figure A3. SEM Images of Commercial NCA (BTR, China) magnified (**a**) 1100× and (**b**) 17336×.

Table A1. Ni-Co-Al molar fraction of Commercial NCA (BTR, China).

Element	mol%
Ni	81.14
Co	17.42
Al	1.44

References

1. Tarascon, J.M.; Armand, M. Issues and challenges facing rechargeable lithium batteries. *Nature* **2001**, *414*, 359–367. [CrossRef]
2. Mizushima, K.; Jones, P.C.; Wiseman, P.J.; Goodenough, J.B. $LixCoO_2$ ($0 < x \leq 1$): A new cathode material for batteries of high energy density. *Solid State Ion.* **1981**, *3–4*, 171–174. [CrossRef]
3. Banza, C.L.N.; Nawrot, T.S.; Haufroid, V.; Decrée, S.; De Putter, T.; Smolders, E.; Kabyla, B.I.; Luboya, O.N.; Ilunga, A.N.; Mutombo, A.M.; et al. High human exposure to cobalt and other metals in Katanga, a mining area of the Democratic Republic of Congo. *Environ. Res.* **2009**, *109*, 745–752. [CrossRef] [PubMed]
4. Purwanto, A.; Yudha, C.S.; Ubaidillah, U.; Widiyandari, H.; Ogi, T. NCA cathode material: Synthesis methods and performance enhancement efforts. *Mater. Res. Express* **2018**, *5*, 122001. [CrossRef]
5. Nitta, N.; Wu, F.; Lee, J.T.; Yushin, G. Li-ion battery materials: Present and future. *Mater. Today* **2015**, *18*, 252–264. [CrossRef]
6. Lai, Y.Q.; Xu, M.; Zhang, Z.A.; Gao, C.H.; Wang, P.; Yu, Z.Y. Optimized structure stability and electrochemical performance of $LiNi_{0.8}Co_{0.15}Al_{0.05}O_2$ by sputtering nanoscale ZnO film. *J. Power Sources* **2016**, *309*, 20–26. [CrossRef]
7. Xia, S.; Zhang, Y.; Dong, P.; Zhang, Y. Synthesis cathode material $LiNi_{0.8}Co_{0.15}Al_{0.05}O_2$ with two step solid-state method under air stream. *Eur. Phys. J. Appl. Phys.* **2014**, *65*, 10401. [CrossRef]

8. Qiu, Z.; Zhang, Y.; Wang, D.; Xia, S. A ternary oxide precursor with trigonal structure for synthesis. *J. Solid State Electrochem.* **2017**, *21*, 3037–3046. [CrossRef]
9. Han, C.J.; Yoon, J.H.; Cho, W.I.; Jang, H. Electrochemical properties of $LiNi_{0.8}Co_{0.2-x}Al_xO_2$ prepared by a sol-gel method. *J. Power Sources* **2004**, *136*, 132–138. [CrossRef]
10. Dong, P.; Xia, S.; Zhang, Y.; Zhang, Y.; Qiu, Z.; Yao, Y. Influence of Complexing Agents on the Structure and Electrochemical Properties of $LiNi_{0.80}Co_{0.15}Al_{0.05}O_2$ Cathode Synthesized by Sol-Gel Method: A Comparative Study. *Int. J. Electrochem. Sci.* **2017**, *12*, 561–575. [CrossRef]
11. Ju, S.H.; Kim, J.H.; Kang, Y.C. Electrochemical properties of $LiNi_{0.8}Co_{0.2-x}Al_xO_2$ ($0 \le x \le 0.1$) cathode particles prepared by spray pyrolysis from the spray solutions with and without organic additives. *Met. Mater. Int.* **2010**, *16*, 299–303. [CrossRef]
12. Park, G.D.; Kang, Y.C. Characteristics of precursor powders of a nickel-rich cathode material prepared by a spray drying process using water-soluble metal salts. *RSC Adv.* **2014**, *4*, 44203–44207. [CrossRef]
13. Yang, H.; Liu, P.; Chen, Q.; Liu, X.; Lu, Y.; Xie, S.; Ni, L.; Wu, X.; Peng, M.; Chen, Y.; et al. Fabrication and characteristics of high-capacity $LiNi_{0.8}Co_{0.15}Al_{0.05}O_2$ with monodisperse yolk–shell spherical precursors by a facile method. *RSC Adv.* **2014**, *4*, 35522–35527. [CrossRef]
14. Kleiner, K.; Melke, J.; Merz, M.; Jakes, P.; Nagel, P.; Schuppler, S.; Liebau, V.; Ehrenberg, H. Unraveling the Degradation Process of $LiNi_{0.8}Co_{0.15}Al_{0.05}O_2$ Electrodes in Commercial Lithium Ion Batteries by Electronic Structure Investigations. *ACS Appl. Mater. Interfaces* **2015**, *7*, 19589–19600. [CrossRef]
15. Seo, J.; Lee, J. Fast growth of the precursor particles of $Li(Ni_{0.8}Co_{0.16}Al_{0.04})O_2$ via a carbonate co-precipitation route and its electrochemical performance. *J. Alloys Compd.* **2017**, *694*, 703–709. [CrossRef]
16. Kim, Y.; Kim, D. Synthesis of High-Density Nickel Cobalt Aluminum Hydroxide by Continuous Coprecipitation Method. *ACS Appl. Mater. Interfaces* **2012**, *4*, 586–589. [CrossRef] [PubMed]
17. Hwang, I.; Lee, C.W.; Kim, J.C.; Yoon, S. Particle size effect of Ni-rich cathode materials on lithium ion battery performance. *Mater. Res. Bull.* **2012**, *47*, 73–78. [CrossRef]
18. Kim, C.; Park, T.-J.; Min, S.-G.; Yang, S.-B.; Son, J.-T. Effects of iron doping at 55 °C on $LiNi_{0.85}Co_{0.10}Al_{0.05}O_2$. *J. Korean Phys. Soc.* **2014**, *65*, 243–247. [CrossRef]
19. Yoo, G.W.; Park, T.J.; Son, J.T. Effect of Structural and Electrochemical Properties of Yttrium-doped $LiNi_{0.90}Co_{0.05}Al_{0.05}O_2$ Electrode by Co - precipitation for Lithium Ion-batteries. *J. New Mater. Electrochem. Syst.* **2015**, *18*, 9–16. [CrossRef]
20. Hua, W.; Zhang, J.; Zheng, Z.; Liu, W.; Peng, X.; Guo, X.-D.; Zhong, B.; Wang, Y.-J.; Wang, X. Na-doped Ni-rich $LiNi_{0.5}Co_{0.2}Mn_{0.3}O_2$ cathode material with both high rate capability and high tap density for lithium ion batteries. *Dalton Trans.* **2014**, *43*, 14824–14832. [CrossRef] [PubMed]
21. Kumar, P.S.; Sakunthala, A.; Rao, R.P.; Adams, S.; Chowdari, B.V.R.; Reddy, M.V. Layered $Li_{1+x}(Ni_{0.33}Co_{0.33}Mn_{0.33})O_2$ cathode material prepared by microwave assisted solvothermal method for lithium ion batteries. *Mater. Res. Bull.* **2017**, *93*, 381–390. [CrossRef]
22. Xie, H.; Hu, G.; Du, K.; Peng, Z.; Cao, Y. An improved continuous co-precipitation method to synthesize $LiNi_{0.80}Co_{0.15}Al_{0.05}O_2$ cathode material. *J. Alloys Compd.* **2016**, *666*, 84–87. [CrossRef]
23. Xie, H.; Du, K.; Hu, G.; Duan, J.; Peng, Z.; Zhang, Z.; Cao, Y. Synthesis of $LiNi_{0.8}Co_{0.15}Al_{0.05}O_2$ with 5-sulfosalicylic acid as a chelating agent and its electrochemical properties. *J. Mater. Chem. A* **2015**, *3*, 20236. [CrossRef]
24. Liu, W.M.; Hu, G.R.; Peng, Z.D.; Du, K.; Cao, Y.B.; Liu, Q. Synthesis of spherical $LiNi_{0.8}Co_{0.15}Al_{0.05}O_2$ cathode materials for lithium-ion batteries by a co-oxidation-controlled crystallization method. *Chin. Chem. Lett.* **2011**, *22*, 1099–1102. [CrossRef]
25. Hu, G.; Liu, W.M.; Peng, Z.; Dua, K.; Cao, Y.B.; Du, K.; Cao, Y.B. Synthesis and electrochemical properties of $LiNi_{0.8}Co_{0.15}Al_{0.05}O_2$ prepared from the precursor $Ni_{0.8}Co_{0.15}Al_{0.05}OOH$. *J. Power Sources* **2012**, *198*, 258–263. [CrossRef]
26. Agarwal, S.; Nekouei, F.; Kargarzadeh, H.; Nekouei, S.; Tyagi, I.; Kumar Gupta, V. Preparation of Nickel hydroxide nanoplates modified activated carbon for Malachite Green removal from solutions: Kinetic, thermodynamic, isotherm and antibacterial studies. *Process Saf. Environ. Prot.* **2016**, *102*, 85–97. [CrossRef]
27. Motlagh, M.M.K.; Youzbashi, A.A.; Sabaghzadeh, L. Synthesis and characterization of Nickel hydroxide/oxide nanoparticles by the complexation-precipitation method. *J. Phys. Sci.* **2011**, *6*, 1471–1476. [CrossRef]

28. Pant, D.; Dolker, T. Green and facile method for the recovery of spent Lithium Nickel Manganese Cobalt Oxide (NMC) based Lithium ion batteries. *Waste Manag.* **2017**, *60*, 689–695. [CrossRef]
29. Subburaj, T.; Jo, Y.N.; Prasanna, K.; Kim, K.J.; Lee, C.W. Titanium oxide nanofibers decorated nickel-rich cathodes as high performance electrodes in lithium ion batteries. *J. Ind. Eng. Chem.* **2017**, *51*, 223–228. [CrossRef]
30. Qiu, Z.; Zhang, Y.; Xia, S.; Yao, Y. A facile method for synthesis of $LiNi_{0.8}Co_{0.15}Al_{0.05}O_2$ cathode material. *Solid State Ion.* **2017**, *307*, 73–78. [CrossRef]
31. Hsieh, C.T.; Hsu, H.H.; Hsu, J.P.; Chen, Y.F.; Chang, J.K. Infrared-assisted Synthesis of Lithium Nickel Cobalt Alumina Oxide Powders as Electrode Material for Lithium-ion Batteries. *Electrochim. Acta* **2016**, *206*, 207–216. [CrossRef]
32. Zhu, J.; Vo, T.; Li, D.; Lu, R.; Kinsinger, N.M.; Xiong, L.; Yan, Y.; Kisalus, D. Crystal Growth of $Li[Ni_{1/3}Co_{1/3}Mn_{1/3}]O_2$ as a Cathode Material for High-Performance Lithium Ion Batteries. *Cryst. Growth Des.* **2012**, *12*, 1118–1123. [CrossRef]
33. Ju, J.-H.; Oh, J.-W.; Cho, S.-W.; Ryu, K.-S.; Kim, G.-O. X-ray absorption spectroscopy studies of the Ni ion of $Li(Ni_{0.8}Co_{0.15}Al_{0.05})_{0.8}(Ni_{0.5}Mn_{0.5})_{0.2}O_2$ with a core–shell structure and $LiNi_{0.8}Co_{0.15}Al_{0.05}O_2$ as cathode materials. *Mater. Res. Bull.* **2012**, *47*, 2830–2833. [CrossRef]
34. Ekawati, K.D.; Sholikah, A.P.; Yudha, C.S.; Widiyandari, H.; Purwanto, A. Comparative Study of NCA Cathode Material Synthesis Methods towards Their Structure Characteristics. In Proceedings of the 2018 5th International Conference on Electric Vehicular Technology (ICEVT), Surakarta, Indonesia, 30–31 October 2018; pp. 57–61. [CrossRef]
35. He, Y. Deterioration mechanism of $LiNi_{0.8}Co_{0.15}Al_{0.05}O_2$/graphite–$SiO_x$ power batteries under high temperature and discharge cycling conditions. *J. Mater. Chem. A Mater. Energy Sustain.* **2017**, *6*, 65–72. [CrossRef]
36. Jian, L.; Bao-Rong, C.; Hong-Ming, Z. Effects of Washing and Heat-treatment on Structure and Electrochemical Charge/Discharge Property for $LiNi_{0.8}Co_{0.15}Al_{0.05}O_2$ Powder. *J. Inorg. Mater.* **2016**, *31*, 773. [CrossRef]
37. He, K.; Ruan, Z.; Teng, X.; Zhu, Y. Facile synthesis and electrochemical properties of spherical $LiNi_{0.85-x}Co_{0.15}Al_xO_2$with sodium aluminate via co-precipitation. *Mater. Res. Bull.* **2017**, *90*, 131–137. [CrossRef]
38. Patnaik, P. Chromatographic Methods. In *Dean's Analytical Chemistry Handbook*; McGraw-Hill: New York, NY, USA, 2004.
39. Park, Y.; Oh, M.; Kim, J.H. Well-dispersed $ZnFe_2O_4$ nanoparticles onto graphene as superior anode materials for lithium ion batteries. *Energies* **2019**, *12*, 304. [CrossRef]
40. Li, H.; Wang, J.; Zhao, Y.; Tan, T. Synthesis of the ZnO@ZnS Nanorod for Lithium-Ion Batteries. *Energies* **2018**, *11*, 2117. [CrossRef]
41. Cheng, T.; Ma, Z.; Gu, R.; Chen, R.; Lyu, Y.; Nie, A.; Guo, B. Cracks Formation in Lithium-Rich Cathode Materials for Lithium-Ion Batteries during the Electrochemical Process. *Energies* **2018**, *11*, 2712. [CrossRef]
42. Kleiner, K.; Dixon, D.; Jakes, P.; Melke, J.; Yavuz, M.; Roth, C.; Nikolowski, K.; Liebau, V.; Ehrenberg, H. Fatigue of $LiNi_{0.8}Co_{0.15}Al_{0.05}O_2$ in commercial Li ion batteries. *J. Power Sources* **2015**, *273*, 70–82. [CrossRef]
43. Zhang, L.; Jiang, J.; Zhang, W. Capacity Decay Mechanism of the LCO + NMC532/Graphite cells combined with post-mortem technique. *Energies* **2017**, *10*, 1147. [CrossRef]